

Rational Spherical Splines For Genus Zero Shape Modeling

Ying He, Xianfeng Gu, Hong Qin

Center for Visual Computing (CVC) and Department of Computer Science
Stony Brook University, Stony Brook, NY, 11794-4400
{yhe|gu|qin}@cs.sunysb.edu

Abstract

Traditional approaches for modeling a closed manifold surface with either regular tensor-product or triangular splines (defined over an open planar domain) require decomposing the acquired geometric data into a group of charts, mapping each chart to a planar parametric domain, fitting an open surface patch of certain degree to each chart, and finally, trimming the patches (if necessary) and stitching all of them together to form a closed manifold. In this paper, we develop a novel modeling method which does not need any cutting or patching operations for genus zero surfaces. Our new approach is founded upon the concept of spherical splines proposed by Pfeifle and Seidel. Our work is strongly inspired by the fact that, for genus zero surfaces, it is both intuitive and necessary to employ spheres as their natural domains. Using this framework, we can convert genus zero mesh to a single rational spherical spline whose maximal error deviated from the original data is less than a user-specified tolerance. With the rational spherical splines, we can model sharp features and edit both the global shape and the local details with ease. Furthermore, we can accurately compute the differential quantities without resorting to any numerical approximations. We conduct several experiments in order to demonstrate the efficacy of our approach for reverse engineering, shape modeling, and interactive graphics.

1. Introduction

With the advent of sophisticated scanning technologies, nowadays we can routinely acquire densely sampled and highly detailed geometric data sets from complicated real-world models. Typically, the acquired digital models are in the form of dense point samples and/or triangular meshes. It is both desirable and necessary to reverse-engineer a spline-based surface from points/meshes for many scientific and industrial applications. By converting dense points/meshes to splines, we will achieve a more compact representa-

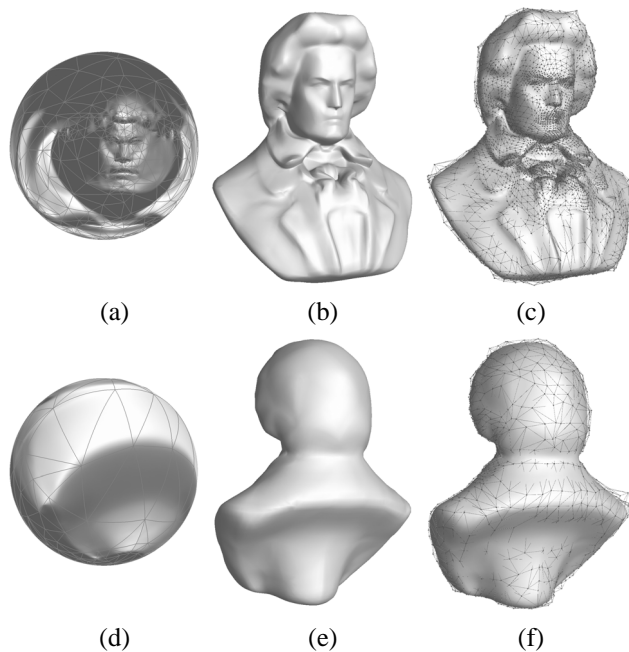


Figure 1. Modeling a genus zero surface using a single rational spherical spline. (a),(d) Spherical parameterization and domain triangulation (1,022 spherical triangles); (b),(e) A C^2 spherical spline; (c),(f) Control net (4,601 control points) overlaid on the spline surface.

tion at different scales in terms of data size, the number of control points, the user-specified threshold error, and other relevant criteria. With a high-order spline formulation, we can accurately compute all the differential quantities such as geodesics, curvatures, and areas without resorting to any numerical approximations via bilinear interpolation and/or local algebraic surface fitting. The rapid and precise evaluations of local and global differential properties will facilitate certain applications such as surface segmentation/classification, shape interrogation, and surface qual-

ity analysis and control. Moreover, a spline-based representation will enable downstream procedures including direct shape modification, free-form deformation, finite element analysis, evaluation, or even digital prototyping.

At present, tensor-product B -spline and NURBS are the prevailing industrial standard for surface representation because of their many attractive geometric properties. Nevertheless, due to their rectangular structures, a single B -spline (and NURBS) patch can represent only simple open surfaces, cylindrical surfaces, or torus-like surfaces. In order to represent surfaces of other topological types without introducing degeneracy, one must define a network of tensor-product B -spline patches and maintain certain continuity between adjacent patches [5, 11].

In shape modeling, many objects are closed-manifold genus zero surfaces, which are topologically equivalent to a sphere. However, most of the commonly-used splines, such as regular tensor-product B -splines and irregular triangular B -splines, are defined on finite open planar domains. In order to model a closed manifold surface, one must cut the scanned data set into a group of charts, mapping each chart to an open planar domain, using a spline patch of certain degree to fit each data chart, and finally stitching all the patches together. This process requires many user interventions and is much more labor intensive and far less intuitive. Therefore, it is imperative to devise a natural and automated way to effectively and accurately model genus zero surfaces using splines without any cutting and patching work. This paper serves this need by formulating rational spherical splines and presenting our prototype system.

Based on the breakthrough work on spherical barycentric coordinates and spherical Bernstein-Bézier (SBB) polynomials by Alfeld, Neamtu and Schumaker [1], Pfeifle and Seidel [14] present scalar spherical triangular B -splines. These splines inherit many properties from their planar counterpart (i.e., planar triangular B -splines), such as the capability of representing any piecewise smooth surfaces of C^{n-1} continuity and modeling the SBB polynomials as a special case. Furthermore, these spherical spline surfaces exhibit no degeneracies that frequently arise when attempting to employ planar parametric spline surfaces for modeling sphere-like, geometrically closed point clouds [14]. Because of the topological equivalence between spheres and other genus zero objects, spherical splines appear to be ideal for modeling closed genus zero surfaces both in theory and in practice.

However, the major drawback of the (non-rational) spherical spline proposed by Pfeifle and Seidel is that it does not satisfy the convex hull property. Therefore, it may be difficult and less intuitive for ordinary users to interactively edit a spline surface by modifying its control net. To make spherical splines more accessible to a broader community and more useful in shape modeling applications,

we present the rational spherical spline which inherits all the attractive properties of Pfeifle and Seidel's spline. More importantly, they offer the convex hull property because of the partition of unity of the rational basis functions. Figure 1 shows an example of modeling a genus zero surface with rational spherical spline. In this paper, we present a general framework to model genus zero surfaces with rational spherical triangular B -splines, which have the following features:

1. The shape is represented in a single degree n spline without any patching and stitching work. The reconstructed surface is C^{n-1} continuous everywhere except at the sharp features.
2. Our surface reconstruction algorithm is based on adaptive conformal spherical parameterization, which has no local distortion and is insensitive to the triangulation and resolution of the input discrete data. The fitting quality can be further improved by enlarging/shrinking any user-specified region on its spherical domain.
3. Based on its compact representation, we can intuitively edit both the overall shape and the details. Also, it is easy to compute the differential properties, such as curvatures, without resorting to any numerical approximations via bilinear interpolation and/or local algebraic surface fitting.

2. Previous Work

2.1. Spherical splines

Defining splines over a sphere has been studied during the past decade. Alfeld et al. [1] present spherical barycentric coordinates which naturally lead to the theory of Spherical Bernstein-Bézier polynomials (SBB). They show fitting scattered data on sphere-like surfaces with SBB in [2]. Pfeifle and Seidel [14] present scalar spherical triangular splines and demonstrate the use of these splines for approximating spherical scattered data. Neamtu [13] constructs a functional space of homogeneous simplex splines and shows that restricting the homogeneous splines to a sphere gives rise to the space of spherical simplex splines. Schröder and Sweldens propose a wavelet construction for scalar functions defined on sphere [16]. Lyche and Schumaker present a multi-resolution method for fitting functions on the sphere [12]. Their method is based on the tensor product of quadratic B -splines and trigonometric splines of order 3, and it produces surfaces which are tangent-plane continuous. Buss and Fillmore present the spherical averages which result in the direct generalization of Bézier and B -spline curves to spherical spline curves [3].

2.2. Spherical parameterization

Parameterization of 3D mesh data is also relevant in shape modeling and interactive graphics applications, including reverse engineering, texture mapping, remeshing, morphing, and scattered data fitting. While planar parameterization has been studied extensively for many years, spherical parameterization remains less investigated. Several algorithms which guarantee a valid spherical embedding exist. Haker et al. [9] introduce an algorithm to conformally map a genus zero surface to the sphere by using the Laplace-Beltrami operator. Gu et al. [8] use harmonic maps to compute spherical conformal parameterizations. Sheffer et al. [17] present a non-linear optimization procedure which deals with the angles of the spherical triangulation. Gotsman et al. [7] show an intrinsic relationship between spectral graph theory and spherical parameterization, and embed meshes on the sphere by solving a quadratic system. Praun and Hoppe [15] present a technique for parameterizing genus zero models onto the sphere using progressive mesh, and introduce several approaches for resampling the spherical signal onto regular domains with simple boundary symmetries.

3. Spherical Triangular B -spline

In this section, we first briefly review the definitions of spherical simplex splines and spherical triangular splines [14]. Then we introduce the rational generalization of the spherical spline and document its key geometric properties for shape modeling.

3.1. Spherical simplex spline

Denote by $\mathbb{S}^2 = \{\mathbf{x} \in \mathbb{R}^3, \|\mathbf{x}\| = 1\}$ a unit sphere in \mathbb{R}^3 . Consider $V = \{\mathbf{t}_0, \dots, \mathbf{t}_{n+2}\} \in \mathbb{S}^2$ on the sphere. Furthermore, select a split set $W = \{\mathbf{t}_{i_0}, \mathbf{t}_{i_1}, \mathbf{t}_{i_2}\} \subset V$. Then, for $n > 0$, the degree n spherical simplex spline $M(\mathbf{u}|V)$ is defined as follows:

$$M(\mathbf{u}|V) = \sum_{j=0}^2 b_j(\mathbf{u}|W)M(\mathbf{u}|V \setminus \{\mathbf{t}_{i_j}\}) \quad (1)$$

where

$$b_0 = \frac{\det(\mathbf{u}, \mathbf{t}_{i_1}, \mathbf{t}_{i_2})}{\det(\mathbf{t}_{i_0}, \mathbf{t}_{i_1}, \mathbf{t}_{i_2})}, b_1 = \frac{\det(\mathbf{t}_{i_0}, \mathbf{u}, \mathbf{t}_{i_2})}{\det(\mathbf{t}_{i_0}, \mathbf{t}_{i_1}, \mathbf{t}_{i_2})}, b_2 = \frac{\det(\mathbf{t}_{i_0}, \mathbf{t}_{i_1}, \mathbf{u})}{\det(\mathbf{t}_{i_0}, \mathbf{t}_{i_1}, \mathbf{t}_{i_2})}$$

are the spherical barycentric coordinates with respect to W . Unlike the planar case, $\sum_{j=0}^2 b_j(\mathbf{u}|W) \geq 1$ if \mathbf{u} lies on or within W .

When $n = 0$, we define

$$M(\mathbf{u}|\mathbf{t}_0, \mathbf{t}_1, \mathbf{t}_2) = \frac{\chi_{[\mathbf{t}_0, \mathbf{t}_1, \mathbf{t}_2]}(\mathbf{u})}{|\det(\mathbf{t}_0, \mathbf{t}_1, \mathbf{t}_2)|} \quad (2)$$

where $\chi_{[\mathbf{t}_0, \mathbf{t}_1, \mathbf{t}_2]}(\mathbf{u})$ is the characteristic function on the half open convex hull of $[\mathbf{t}_0, \mathbf{t}_1, \mathbf{t}_2)$.

As was the case with triangular B -splines, the directional derivative of $M(\mathbf{u}|V)$ along a vector \mathbf{v} (perpendicular to \mathbf{u}) can also be computed recursively as:

$$D_{\mathbf{v}}M(\mathbf{u}|V) = n \sum_{j=0}^2 b_j(\mathbf{v}|W)M(\mathbf{u}|V \setminus \{\mathbf{t}_{i_j}\}) \quad (3)$$

3.2. Spherical triangular spline space

The spherical triangular spline can be constructed in a similar way as the planar triangular B -spline [4]. In the interest of page limitation, we only discuss its construction briefly: let points $\mathbf{t}_i \in \mathbb{S}^2$, $i \in \mathbb{N}$, be given and define a spherical triangulation

$$T = \{\Delta(I) = [\mathbf{t}_{i_0}, \mathbf{t}_{i_1}, \mathbf{t}_{i_2}] : I = (i_0, i_1, i_2) \in I \subset \mathbb{N}^3\},$$

where every triangle is oriented counter-clockwise (or clockwise). Next, with every vertex \mathbf{t}_i of T we associate a cloud of knots $\mathbf{t}_{i,0}, \dots, \mathbf{t}_{i,n}$ such that $\mathbf{t}_{i,0} = \mathbf{t}_i$. To clarify the notations, we call $\mathbf{t}_{i,0}$ the primary knot and $\mathbf{t}_{i,j}$, $1 \leq j \leq n$ the sub-knots. For every spherical triangle $I = [\mathbf{t}_{i_0}, \mathbf{t}_{i_1}, \mathbf{t}_{i_2}] \in T$,

1. all the triangles $X_{\beta}^I = [\mathbf{t}_{i_0, \beta_0}, \mathbf{t}_{i_1, \beta_1}, \mathbf{t}_{i_2, \beta_2}]$ with $\beta = (\beta_0, \beta_1, \beta_2)$ and $|\beta| = \beta_0 + \beta_1 + \beta_2 \leq n$ are non-degenerate.

2. the set

$$\Omega_n^I = \text{interior}(\cap_{|\beta| \leq n} X_{\beta}^I)$$

satisfies

$$\Omega_n^I \neq \emptyset. \quad (4)$$

Then the spherical triangular B -spline basis function N_{β}^I , $|\beta| = n$, is defined by means of spherical simplex splines $M(\mathbf{u}|V_{\beta}^I)$ as

$$N(\mathbf{u}|V_{\beta}^I) = |\det(X_{\beta}^I)|M(\mathbf{u}|V_{\beta}^I)$$

where $V_{\beta}^I = \{\mathbf{t}_{i_0,0}, \dots, \mathbf{t}_{i_0, \beta_0}, \dots, \mathbf{t}_{i_2,0}, \dots, \mathbf{t}_{i_2, \beta_2}\}$.

A degree n spherical triangular B -spline surface \mathbf{F} over T is then defined as

$$\mathbf{F}(\mathbf{u}) = \sum_{I \in T} \sum_{|\beta|=n} \mathbf{c}_{I, \beta} N(\mathbf{u}|V_{\beta}^I). \quad (5)$$

where $\mathbf{c}_{I, \beta} \in \mathbb{R}^3$ are the control points.

Figure 2(a) shows a quadratic spherical spline patch defined on $\{\mathbf{t}_0, \mathbf{t}_1, \mathbf{t}_2\}$. We associate two sub-knots $\mathbf{t}_{i,j}$, $j = 1, 2$ to each vertex \mathbf{t}_i . The six basis functions are shown in Figure 2(b)-(g). Since no three knots are co-circular, every basis function is C^1 everywhere.

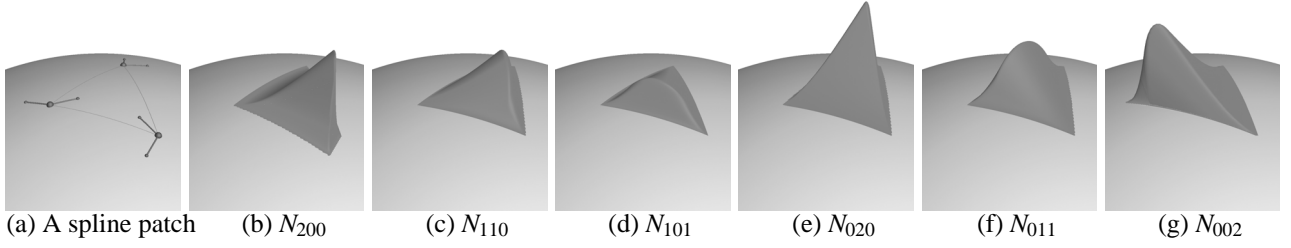


Figure 2. Six basis functions of a quadratic spherical spline patch.

3.3. Rational Spherical Spline

Despite many attractive properties for shape modeling, one key drawback of spherical triangular B -splines is that their control points do not lend themselves to an intuitive and natural geometric “handler” of the underlying shape for convenient free-form shape editing, i.e., the convex hull property does not hold. This deficiency results from the fact that the spherical barycentric coordinate does not yield partition of unity, since $\sum_{j=0}^2 b_j(\mathbf{u}|W) \geq 1$. Thus, $\sum_{I \in T} \sum_{|\beta|=n} N_{\beta}^I(\mathbf{u}|V_{\beta}^I) \geq 1$ for every $\mathbf{u} \in \mathbb{S}^2$.

To further improve spherical splines, we present their rational generalization:

$$\mathbf{F}(\mathbf{u}) = \frac{P(\mathbf{u})}{Q(\mathbf{u})} = \frac{\sum_{I \in T} \sum_{|\beta|=n} \omega_{I,\beta} \mathbf{c}_{I,\beta} N(\mathbf{u}|V_{\beta}^I)}{\sum_{I \in T} \sum_{|\beta|=n} \omega_{I,\beta} N(\mathbf{u}|V_{\beta}^I)}. \quad (6)$$

where $\omega_{I,\beta} \in \mathbb{R}^+$ are the weights.

Because of partition of unity, rational spherical splines satisfy the convex hull property. More importantly, by introducing the non-negative weights, we have more degree of freedom to control the spline shape. Figure 11 illustrates the influence of different weights on a model for shape control.

For a general rational spherical spline surface, each triangle I has its own set of control points $\mathbf{c}_{I,\beta}$ and weights $\omega_{I,\beta}$. However, in this paper we consider a more restricted class of surfaces by sharing respective control points and weights along common boundaries of two adjacent triangles in the parametric triangulation.

For spherical splines with shared control points/weights, we can prove

$$P(\mathbf{u}) = \sum_{I \in T} \sum_{|\beta|=n-1} \mathbf{c}_{I,\beta}^{(1)}(\mathbf{u}) N(\mathbf{u}|V_{\beta}^I) \quad (7)$$

$$Q(\mathbf{u}) = \sum_{I \in T} \sum_{|\beta|=n-1} \omega_{I,\beta}^{(1)}(\mathbf{u}) N(\mathbf{u}|V_{\beta}^I) \quad (8)$$

where

$$\mathbf{c}_{I,\beta}^{(1)}(\mathbf{u}) = \sum_{j=0}^2 \mathbf{c}_{I,\beta+e^j} \omega_{I,\beta+e^j} b_j(\mathbf{u}|X_{\beta}^I)$$

$$\omega_{I,\beta}^{(1)}(\mathbf{u}) = \sum_{j=0}^2 \omega_{I,\beta+e^j} b_j(\mathbf{u}|X_{\beta}^I).$$

and $e^j = (\delta_{j,i})_{i=0}^2$, $j = 0, 1, 2$ are the coordinate vectors. Here, $\mathbf{c}_{I,\beta}^{(1)}(\mathbf{u})$ and $\omega_{I,\beta}^{(1)}(\mathbf{u})$ are also called virtual control points and weights. Therefore, a degree n rational spherical spline $\mathbf{F}(\mathbf{u}) = P(\mathbf{u})/Q(\mathbf{u})$ can be evaluated with the efficiency of a degree $n-1$ spline. In practice, this property is very useful to improve the performance of the evaluation algorithm.

Similarly, the directional derivative along the direction \mathbf{v} can be calculated as follows:

$$D_{\mathbf{v}}\mathbf{F}(\mathbf{u}) = \frac{D_{\mathbf{v}}P(\mathbf{u}) - \mathbf{F}(\mathbf{u})D_{\mathbf{v}}Q(\mathbf{u})}{Q(\mathbf{u})} \quad (9)$$

where

$$D_{\mathbf{v}}P(\mathbf{u}) = n \sum_{I \in T} \sum_{|\beta|=n-1} \mathbf{c}_{I,\beta}^{(2)}(\mathbf{v}) N(\mathbf{u}|V_{\beta}^I) \quad (10)$$

$$D_{\mathbf{v}}Q(\mathbf{u}) = n \sum_{I \in T} \sum_{|\beta|=n-1} \omega_{I,\beta}^{(2)}(\mathbf{v}) N(\mathbf{u}|V_{\beta}^I) \quad (11)$$

and

$$\mathbf{c}_{I,\beta}^{(2)}(\mathbf{v}) = \sum_{j=0}^2 \mathbf{c}_{I,\beta+e^j} b_j(\mathbf{v}|X_{\beta}^I)$$

$$\omega_{I,\beta}^{(2)}(\mathbf{v}) = \sum_{j=0}^2 \omega_{I,\beta+e^j} b_j(\mathbf{v}|X_{\beta}^I).$$

Note that $\mathbf{F}(\mathbf{u})$ and $D_{\mathbf{v}}\mathbf{F}(\mathbf{u})$ share the same basis functions. Thus, the value $\mathbf{F}(\mathbf{u})$ and the first order derivatives can be evaluated in a unified way, with a minimal extra cost.

We modify and extend Franssen et al. [6]’s evaluation algorithm on planar triangular B -splines to a spherical setting. For each parameter $\mathbf{u} \in \mathbb{S}^2$, we first locate the spherical triangle I containing \mathbf{u} and calculate the basis functions $N(\mathbf{u}|V_{\beta}^I)$ for triangle I and its 1-ring neighbors. Then we choose two orthogonal vectors \mathbf{v}_1 and \mathbf{v}_2 such that \mathbf{u} ,

\mathbf{v}_1 and \mathbf{v}_2 form a local coordinate system. Next, we calculate the virtual control points and weights, $\mathbf{c}_{I,\beta}^{(1)}(\mathbf{u})$, $\omega_{I,\beta}^{(1)}(\mathbf{u})$, $\mathbf{c}_{I,\beta}^{(2)}(\mathbf{v})|_{\mathbf{v}=\mathbf{v}_1,\mathbf{v}_2}$, and $\omega_{I,\beta}^{(2)}(\mathbf{v})|_{\mathbf{v}=\mathbf{v}_1,\mathbf{v}_2}$. Finally, we can compute the value of \mathbf{F} and the normal $D_{\mathbf{v}_1}\mathbf{F}(\mathbf{u}) \times D_{\mathbf{v}_2}\mathbf{F}(\mathbf{u})$ using Equations (7) and (10).

3.4. Properties of Spherical Spline

The rational spherical triangular B -spline shares many properties with its planar counterpart, including:

- *Piecewise rational polynomial*: $\mathbf{F}(\mathbf{u})$ is a piecewise rational polynomial of degree n defined on the sphere.
- *Locality*: The movement of a single control point $\mathbf{c}_{I,\beta}$ only influences the surface on the triangle I and on the triangles directly surrounding I .
- *Smoothness*: If the knots of each set V_β^I are in ‘‘spherical’’ general position (i.e., no three knots in V_β^I lie on the same great circle), then $\mathbf{F}(\mathbf{u})$ is C^{n-1} continuous everywhere.
- *Convex Hull*: $\mathbf{F}(\mathbf{u})$ lies inside the convex hull of its control net. The non-negative weights also provide extra degrees of freedom to control the spline shape.

4. Surface Approximation Algorithm

4.1. Overview

We now discuss the problem of finding a good approximation of a given set of points $P = \{\mathbf{p}_i\}_{i=1}^m$ by a rational spherical triangular spline. In this paper, we assume that these data form a closed manifold genus-zero surface.

A commonly-used technology is to minimize a linear combination of interpolation and fairness functionals, i.e.,

$$\min E = E_{dist} + \lambda E_{fair}. \quad (12)$$

The first part is

$$E_{dist} = \sum_{i=1}^m \|\mathbf{F}(\mathbf{u}_i) - \mathbf{p}_i\|^2$$

where $\mathbf{u}_i \in \mathbb{S}^2$ is the parameter for \mathbf{p}_i , $i = 1, \dots, m$.

The second part E_{fair} in (12) is a smoothing term. Two frequently used examples are the membrane energy and thin plate energy,

$$E_{fair} = \iint_{\mathbb{S}^2} (\mathbf{F}_u^2 + \mathbf{F}_v^2) dudv,$$

$$E_{fair} = \iint_{\mathbb{S}^2} (\mathbf{F}_{uu}^2 + 2\mathbf{F}_{uv}^2 + \mathbf{F}_{vv}^2) dudv,$$

where u and v are spherical coordinates of $\mathbf{u} \in \mathbb{S}^2$, i.e., $\mathbf{u} = (\cos(u)\sin(v), \sin(u)\sin(v), \cos(v))^T$, $u \in [0, 2\pi)$, $v \in [0, \pi]$.

Both parts are quadratic functions of the unknown control points.

The pseudo code of our algorithm is as follows:

```

1. Perform adaptive spherical conformal
   parameterization (Sec. 4.2).
2. Construct the initial domain
   triangulation (Sec. 4.3).
3. while max  $\|\mathbf{p}_i - \mathbf{F}(\mathbf{u}_i)\| > \epsilon, i = 1, \dots, m$ 
4.   Compute the control points (Sec. 4.4).
5.   Parameter correction (Sec. 4.5).
6.   Adaptive refinement (Sec. 4.6).
7. end

```

We further illustrate the pipeline with the example of David’s head as shown in Figure 3.

4.2. Adaptive conformal spherical parameterization

In this step we construct an invertible mapping between the surface and the unit sphere. We use the conformal spherical parameterization, as introduced in [8]. Conformal parameterization has no local distortion and is suitable for texture mapping spline surfaces. In terms of computation on manifolds, conformal parameterization introduces the simplest Riemannian metric form (also differential operators). This will simplify the computation. More importantly, conformal parameterization is insensitive to triangulation and resolution, and similar geometries induce similar conformal spherical parameterizations. Therefore, such a parameterization is also valuable for reverse engineering, where the quality of surface reconstruction hinges upon the mapping between the data input and the spline-modeled surface.

There are infinite spherical parameterizations for a given surface. Different parameterizations affect the quality of the result spherical spline surfaces. Suppose a spherical parameterization of surface M is $\phi : M \rightarrow \mathbb{S}^2$, and $\tau : \mathbb{S}^2 \rightarrow \mathbb{S}^2$ is an automorphism of \mathbb{S}^2 (a one-to-one differential map from the unit sphere to itself), then $\tau \circ \phi$ is also a spherical parameterization of M . In our current work, we use a subset of the automorphism group of \mathbb{S}^2 , the so called Möbius transformation group, then τ is a Möbius transformation.

Suppose $\zeta : \mathbb{S}^2 \rightarrow \mathbb{C}$ is the stereo-graphic projection,

$$\zeta(x, y, z) = \left(\frac{x}{1-z}, \frac{y}{1-z} \right), \quad (13)$$

A Möbius transformation for the complex plane is

$$\gamma(z) = \frac{az+b}{cz+d}, ad-bc=1, a, b, c, d \in \mathbb{C}. \quad (14)$$

Any spherical Möbius transformation can be reprinted as $\zeta^{-1} \circ \gamma \circ \zeta$.

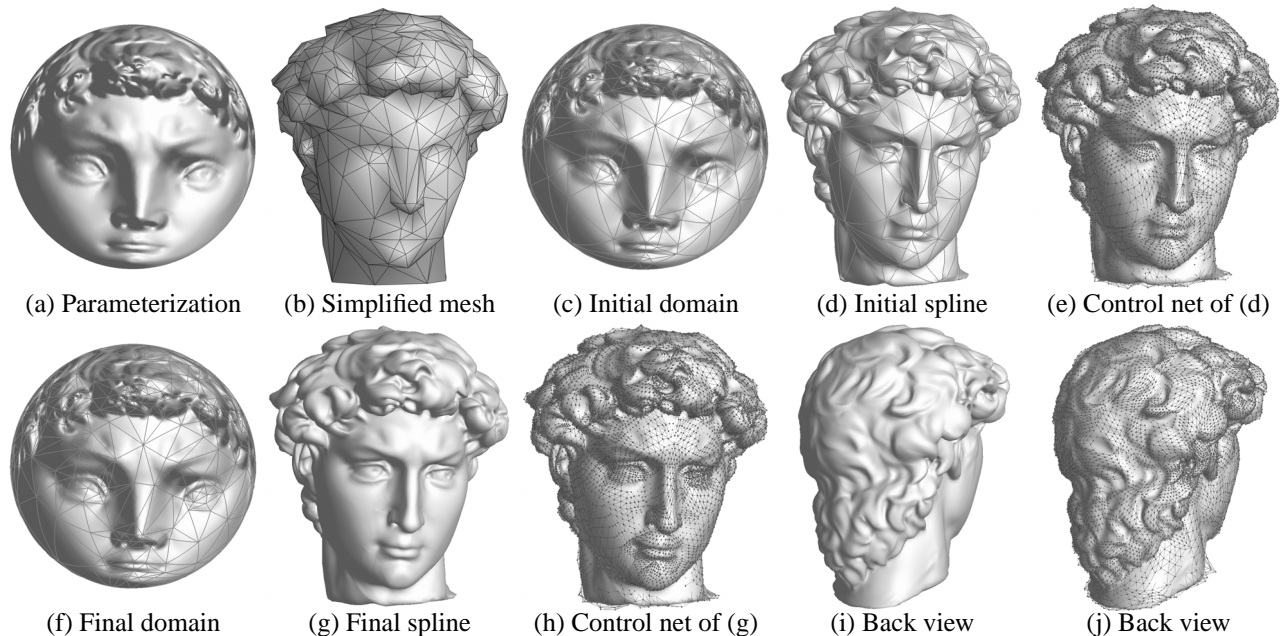


Figure 3. Illustration of surface reconstruction using spherical splines. (a) Conformal spherical parameterization. (b) Simplified mesh with 1,000 triangles. (c) Map (b) to the sphere. (d) A degree 5 spherical spline defined on (c), r.m.s. error 0.07%. (e) The control net of (d), 12,502 control points. (f) Adaptively refined domain triangulation with 1,236 spherical triangles. (g) Reconstructed spline based on (f), r.m.s. error 0.04%. (h) Control net of (g), 15,452 control points. (i-j) Back view.

First we compute one specific spherical parameterization ϕ , then by composing with different spherical Möbius transformations, we can adapt the parameterization to the purpose of the spline fitting. Figure 4 shows an example of adaptive conformal spherical parameterization. In the original parameterization, the Isis’s head shrinks to a small area (Figure 4(a)), which causes difficulties in reconstruction due to fewer domain triangles in that area. Using the above adaptive conformal spherical parameterization method, we can enlarge the head area (Figure 4(b)) by a Möbius transformation. With more domain triangles and control points, we can reconstruct the head more accurately (Figure 5(a)&(b)).

4.3. Construct the domain triangulation

In this step we seek to generate an appropriate triangulation of the sphere \mathbb{S}^2 . A naive method is to construct the domain triangulation uniformly, i.e., the vertices are placed “uniformly” (equidistantly) on the sphere and each triangle has roughly the same area. However, this scheme does not yield good results in practice since the parameters $\{\mathbf{u}_i\}_{i=1}^m$ are not distributed uniformly on the sphere. One principle in constructing such a triangulation is that each triangle should contain a similar number of parameter points, i.e., more tri-

angles are needed in the area with denser features and *vice versa*. In this paper, we present an effective method to construct the domain triangulation. Note that one advantage of conformal parameterization is its insensitivity to the triangulation and resolution of the model, i.e., similar geometries induce similar conformal spherical parameterizations. Based on these observations, we first simplify the original model (dense mesh) with a user-specified number of faces. Then we perform conformal spherical parameterization on this simplified model and use this parameterization as the initial domain triangulation. Figure 3(a) shows the parameterization of the David’s head model. Figure 3(b) shows the simplified mesh with 1,000 triangles. We then map the simplified mesh to the sphere as shown in Fig 3(c). Note that this domain triangulation roughly represents the original geometry.

4.4. Compute the control points

We solve Equation 12 for the unknown of control points and weights by Conjugate Gradient method. The value and gradient of the interpolation functional can be computed straightforwardly. However, it is difficult to calculate the exact value of the fair functional and the corresponding gradients. In our implementation, we use the thin-plate energy

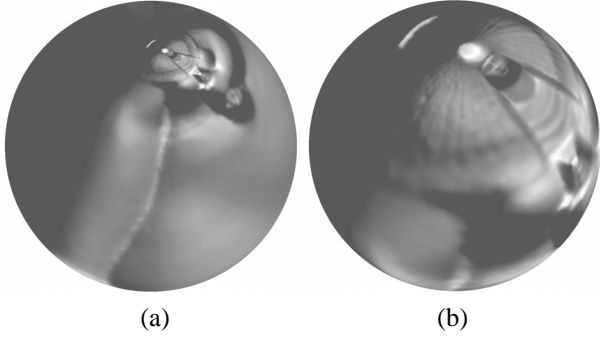


Figure 4. Adaptive conformal spherical parameterization. (a) Original conformal spherical parameterization. It is difficult to reconstruct the details of the head based on (a) due to the corresponding small area on the sphere. (b) Enlarging the head part using a Möbius transformation.

as the fair functional. For each spherical triangle I , we uniformly split it to a user-specified number of patches (400 in our experiments, i.e., Δ_i^j , $i = 1, \dots, 400$). Denote by \mathbf{u}_i^j the centroid of Δ_i^j and s_i^j the area of Δ_i^j . Then we linearize the integral as

$$E_{fair} \approx \sum_I \sum_i (\mathbf{F}_{uu}^2(\mathbf{u}_i^j) + 2\mathbf{F}_{uv}^2(\mathbf{u}_i^j) + \mathbf{F}_{vv}^2(\mathbf{u}_i^j)) s_i^j.$$

The second order derivative of \mathbf{F} with respect to control points and weights can be calculated analytically. We set the initial fairness factor $\lambda = 0.01$ in our experiments and decrease the value gradually during the fitting iteration.

4.5. Parameter correction

It is well known that the parameter choice critically affects the fitting result. Therefore, we utilize a parameter correction procedure in the pipeline. The standard method, introduced by Hoschek in [10], is derived from the observation that the error $\mathbf{p}_i - \mathbf{F}(\mathbf{u}_i)$ will not be orthogonal with respect to the approximating surface in general and will thus not represent the minimal distance between the surface and the data point. If that happens, the parameter value \mathbf{u}_i should be corrected. This is done by minimizing the following objective function

$$\min D_i(\mathbf{u}) = \|\mathbf{F}(\mathbf{u}) - \mathbf{p}_i\|^2 \quad (15)$$

for each sample \mathbf{p}_i . In our implementation, we use Newton method to solve this problem.

Object	#points	n	N_t	N_c	<i>r.m.s</i>
Beethoven	40,000	3	1,022	4,601	0.02%
David	203,219	5	1,236	15,452	0.03%
Dog	195,586	5	472	5,902	0.01%
Isis	187,644	4	540	4,322	0.02%
Teeth	116,604	4	554	4,434	0.007%

Table 1. Spline configuration. n , degree of spherical splines; N_t , # of domain triangles; N_c , # of control points; *r.m.s.*, root mean square error.

4.6. Adaptive refinement

In our method, we control the quality of the spherical spline by specifying the maximal fitting tolerance $L_\infty = \max \|\mathbf{F}(\mathbf{u}_i) - \mathbf{p}_i\|$, $i = 1, \dots, m$ (We set $L_\infty = 0.1\%$ of the diagonal of the object in our experiments). If the current surface does not satisfy this criterion, we employ adaptive refinement to introduce new degrees of freedom into the surface representation to improve the fitting quality. Suppose triangle I violates the criterion and denote L_∞^I the L_∞ error on triangle I . If the $L_\infty^I > 2\epsilon$, split the triangle I using 1-to-4 scheme and then split the neighboring triangles to avoid T-junctions; Otherwise, we split the longest edge.

After adaptive refinement, we then repeat the fitting procedure until the maximal fitting tolerance is satisfied. The reconstructed David’s head is shown in Figure 3(f)-(j). The refined domain has 1,236 triangles and 15,452 control points. The root-mean-square (r.m.s.) error is 0.03%.

5. Results & Applications

We have implemented a prototype system on a 3GHz Pentium IV PC with 1GB RAM. We perform experiments on various closed genus zero surfaces from sphere-like surfaces, such as David’s head, teeth, to surfaces with long extruding parts, such as Isis. In order to compare the fitting error across different models, we uniformly scale the models to fit within a unit cube. Table 1 shows the spline complexities. By converting dense meshes to spherical splines, we achieve a compact representation, high continuity and small approximation error.

5.1. Editing the details

We can easily edit the details by adding a separate scalar spherical spline to the existing base one. Figure 5 shows an example of embossing on the Isis model. We first sketch a flower on the sphere. Next, we construct a scalar spherical spline $D(\mathbf{u})$ and enhance its control points according to the sketch. Finally, we evaluate the scalar spline as the dis-

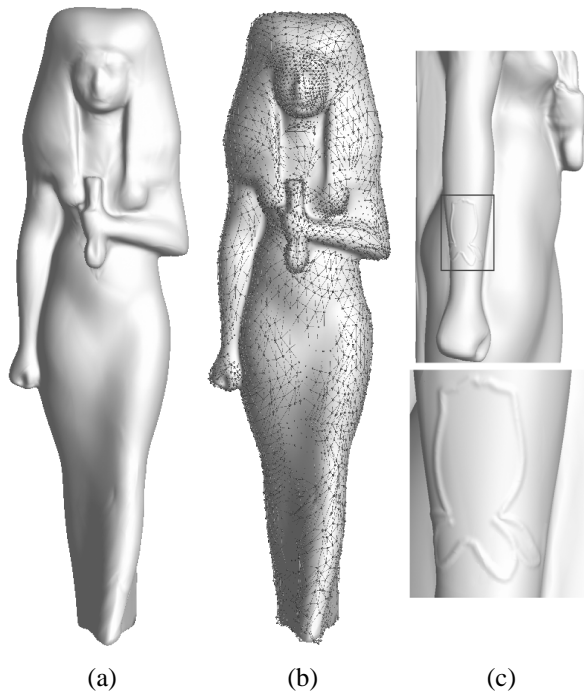


Figure 5. Editing the details on the spherical spline. (a) A degree 4 spherical spline. (b) 4,402 control points. (c) We sketch another scalar spherical spline on (a).

placement and add it to the original spline $\mathbf{F}(\mathbf{u})$, i.e., the modified spline $\tilde{\mathbf{F}}(\mathbf{u})$ can be evaluated as follows:

$$\tilde{\mathbf{F}}(\mathbf{u}) = \mathbf{F}(\mathbf{u}) + D(\mathbf{u})\mathbf{F}_{\mathbf{v}_1}(\mathbf{u}) \times \mathbf{F}_{\mathbf{v}_2}(\mathbf{u}) \quad (16)$$

where \mathbf{v}_1 , \mathbf{v}_2 and \mathbf{u} form a local coordinate system at \mathbf{u} .

5.2. Editing the control net

As shown in Figure 6(b), the dog model is reconstructed by a degree 5 spherical spline containing 5,902 control points (Figure 6(a)). We deform the control net (Figure 6(c)), and obtain the deformed spline (Figure 6(d)).

5.3. Computing the differential properties

One key advantage of the spline based representation is that we have the analytical form of the underlying shape. Thus, we can compute the normals, curvatures, geodesic, areas, etc., anywhere on the surface. Figure 8 shows the mean curvature and principal direction on the dog model.

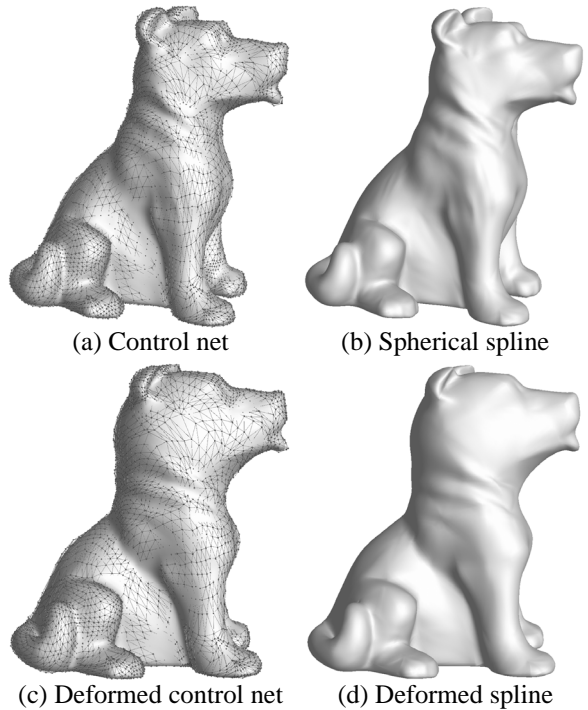


Figure 6. Editing the control net. (a)&(b) A degree 5 spherical spline. We deform the control net and re-evaluate the spline. (c)&(d) Deformed control net and spline surface.

5.4. Modeling features

Although it is desirable in principle to have surfaces that are as smooth as possible, in practice it is necessary to be able to model discontinuities like sharp edges or corners as well. We know that the rational spherical spline is globally C^{n-1} continuous if the knots are in “spherical” general position (Section 3.4). However, we can model sharp features by intentionally placing knots co-circularly. Figure 9 shows an example of modeling features on the teeth model. Benefiting from the conformal spherical parameterization, the sharp features on the original model can be faithfully mapped to the sphere. Therefore, by constructing the domain triangulation according to the features and place the knots along the desired knot lines, we can model the features easily and accurately in one single representation.

6. Discussion

A degree n spherical triangular B -spline has globally C^{n-1} continuity if there are no degenerate knots. However, in some cases, there exist some so-called “knot-lines” where the corresponding curvatures are larger than other regions.

For example, Figure 10(a) and (b) show a degree 5 spherical triangular B -spline and the mean curvature respectively. These knot lines are the images of the edges in the domain triangulation. Therefore, we can eliminate these knot lines by adjusting the control points and weights. Denote by L the set of edges in the domain triangulation which corresponds to the knot lines. We minimize the integral of principal curvature along the lines in L :

$$\min \int_L \sum_{i,j} \left(\frac{\partial k_i}{\partial u_j} \right)^2 \quad (17)$$

where k_1, k_2 are the principal curvature and u_1, u_2 represent u and v . Note that we fix the control points and only allow the weights to be free variable in Equation 17. Therefore, it results in small changes in the overall shape, but the curvature distribution improves significantly as shown in Figure 10(c) and (d).

7. Conclusion

We have proposed a new shape modeling paradigm for genus zero surfaces based on the concept and formulation of rational spherical triangular B -splines. This new spline scheme utilizes a sphere as its parametric domain, making it fundamentally different from other popular splines defined over open planar domains. As a result, spherical splines appear to be ideal for the effective representation of genus zero closed surfaces without any cutting, trimming, and patching operations. After presenting the theory of rational spherical splines, we have articulated a computational framework to convert genus zero mesh to a single rational spherical spline whose maximal error is less than the user-specified value. Our reverse engineering algorithm is based on adaptive conformal spherical parameterization, which has less local distortion and is insensitive to the triangulation and resolution of the geometric data input. Benefiting from the closed-form analytical formulation of any modeled spline surfaces, we have also developed the modeling toolkits for interactive editing, feature transfer, shape deformation, and shape analysis. Our experiments demonstrate both the efficacy and the accuracy of spherical splines in reverse engineering, intuitive deformation, and shape modeling, especially for genus zero surfaces.

Acknowledgements

This work was supported in part by the NSF grants IIS-0082035 and IIS-0097646, and an Alfred P. Sloan Fellowship to H. Qin and the NSF CAREER Award CCF-0448339 to X. Gu. The models are courtesy of Cyberware, Stanford University and New York University.

References

- [1] P. Alfeld, M. Neamtu, and L. L. Schumaker. Bernstein-bézier polynomials on spheres and sphere-like surfaces. *Computer Aided Geometric Design*, 13(4):333–349, 1996.
- [2] P. Alfeld, M. Neamtu, and L. L. Schumaker. Fitting scattered data on sphere-like surfaces using spherical splines. *J. Comput. Appl. Math.*, 73(1-2):5–43, 1996.
- [3] S. R. Buss and J. P. Fillmore. Spherical averages and applications to spherical splines and interpolation. *ACM Trans. Graph.*, 20(2):95–126, 2001.
- [4] W. Dahmen, C. A. Micchelli, and H.-P. Seidel. Blossoming begets B -spline bases built better by B -patches. *Mathematics of Computation*, 59(199):97–115, 1992.
- [5] M. Eck and H. Hoppe. Automatic reconstruction of b-spline surfaces of arbitrary topological type. In *Proceedings of SIGGRAPH 96*, pages 325–334, 1996.
- [6] M. Franssen, R. C. Veltkamp, and W. Wesselink. Efficient evaluation of triangular B -spline surfaces. *Computer Aided Geometric Design*, 17(9):863–877, 2000.
- [7] C. Gotsman, X. Gu, and A. Sheffer. Fundamentals of spherical parameterization for 3d meshes. *Proceedings of SIGGRAPH 03*, pages 358–363, 2003.
- [8] X. Gu, Y. Wang, T. F. Chan, P. M. Thompson, and S.-T. Yau. Genus zero surface conformal mapping and its application to brain surface mapping. In *Proceedings of Information Processing in Medical Imaging*, pages 172–184, 2003.
- [9] S. Haker, S. Angenent, A. Tannenbaum, R. Kikinis, G. Sapiro, and M. Halle. Conformal surface parameterization for texture mapping. *IEEE Transactions on Visualization and Computer Graphics*, 6(2):181–189, April-June 2000.
- [10] J. Hoschek. Intrinsic parametrization for approximation. *Computer Aided Geometric Design*, 5(1):27–31, 1988.
- [11] V. Krishnamurthy and M. Levoy. Fitting smooth surfaces to dense polygon meshes. In *Proceedings of SIGGRAPH 96*, pages 313–324, 1996.
- [12] T. Lyche and L. L. Schumaker. A multiresolution tensor spline method for fitting functions on the sphere. *SIAM J. Sci. Comput.*, 22(2):724–746, 2000.
- [13] M. Neamtu. Homogeneous simplex splines. *J. Comput. Appl. Math.*, 73(1-2):173–189, 1996.
- [14] R. Pfeifle and H.-P. Seidel. Spherical triangular B -splines with application to data fitting. *Computer Graphics Forum*, 14(3):89–96, 1995.
- [15] E. Praun and H. Hoppe. Spherical parameterization and remeshing. *Proceedings of SIGGRAPH 03*, pages 340–349, 2003.
- [16] P. Schröder and W. Sweldens. Spherical wavelets: efficiently representing functions on the sphere. In *Proceedings of SIGGRAPH 95*, pages 161–172, 1995.
- [17] A. Sheffer, C. Gotsman, and N. Dyn. Robust spherical parameterization of triangular meshes. In *4th Israel-Korea Bi-National Conference on Geometric Modeling and Computer Graphics*, pages 94–99, 2003.

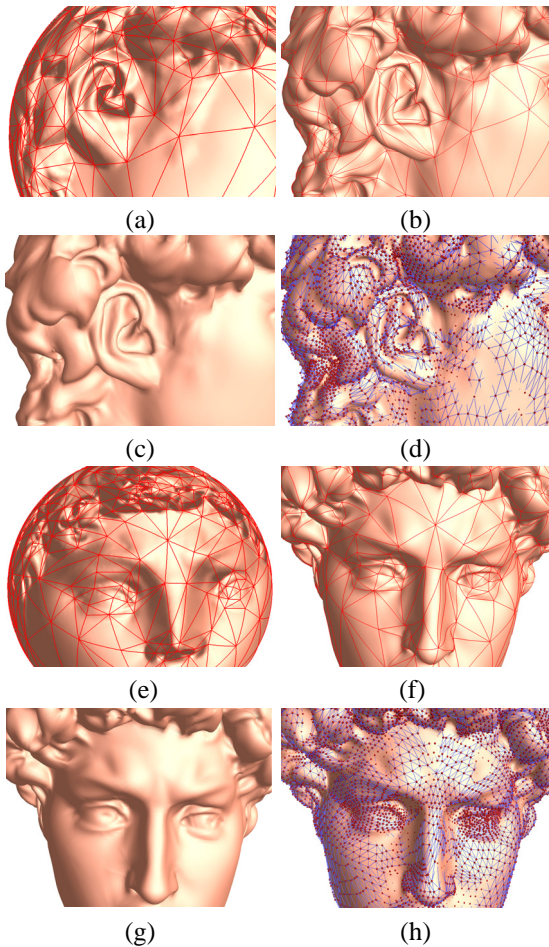


Figure 7. Close-up of the reconstructed David's head model. (a),(e) Spherical triangulation; (b),(f) The red curves on the spline correspond to the edges of domain triangulation; (c),(g) Spline surface; (d),(h) Spline overlaid with control points.

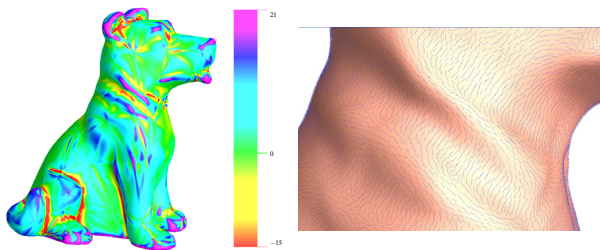


Figure 8. Computing the differential properties. *Left*: Mean curvature; *Right*: Principal direction of k_{min} .

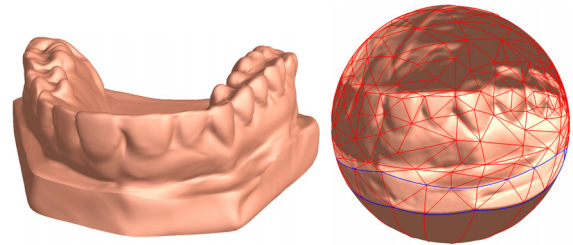


Figure 9. Modeling features by degenerate knots. *Left*: A degree 4 spherical spline is C^3 continuous everywhere except at the features (at the base) which is C^0 ; *Right*: Spherical parametrization and domain triangulation. The knots associated to the vertices on the blue lines are degenerate.

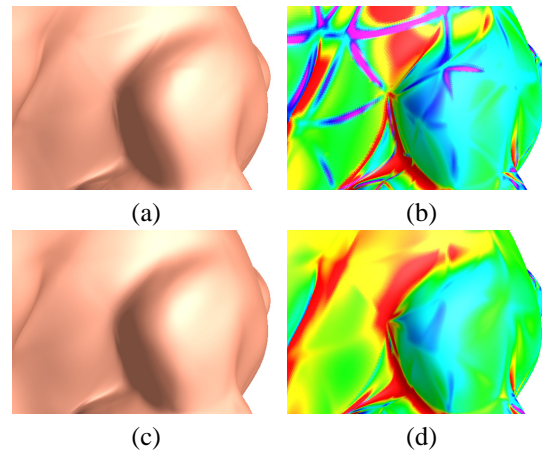


Figure 10. Knot-line elimination. (a)-(b) A degree 5 spherical spline and its mean curvature; (c)-(d) Spline surface after knot line elimination and mean curvature distribution.

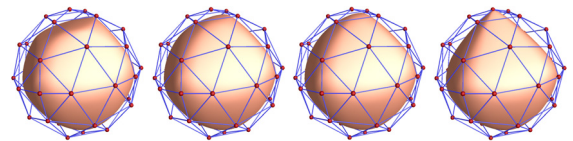


Figure 11. Non-negative weights provide more degree of freedom to control the spline shape. From left to right, the weight of the top-most control point is set to 0, 0.5, 1 and 10, respectively. Other weights are set to 1.